NACA

RESEARCH MEMORANDUM

AERODYNAMIC CHARACTERISTICS OF A WING WITH QUARTER-CHORD LINE SWEPT BACK 45°, ASPECT RATIO 4, TAPER RATIO 0.6, AND NACA 65A006 AIRFOIL SECTION

TRANSONIC-BUMP METHOD

By

Joseph Weil and Kenneth W. Goodson

Langley Aeronautical Laboratory
Langley Air Force Base, Va.

NATIONAL ADVISORY COMMITTEE
FOR AERONAUTICS

WASHINGTON

February 24, 1949
Declassified September 27, 1954

NACA RM No. L9A21

NATIONAL ADVISORY COMMITTEE FOR AERONAUTICS

RESEARCH MEMORANDUM

AERODYNAMIC CHARACTERISTICS OF A WING WITH QUARTER-CHORD LINE SWEPT BACK 45°, ASPECT RATIO 4, TAPER RATIO 0.6, AND NACA 65A006 AIRFOIL SECTION

TRANSONIC-BUMP METHOD

By Joseph Weil and Kenneth W. Goodson

SUMMARY

As part of an NACA transonic research program, a series of wing-body combinations are being investigated in the Langley high-speed 7- by 10-foot tunnel up to a Mach number of 1.18 utilizing the transonic bump.

This paper presents the results of the investigation of a wing-fuselage combination employing a wing with the quarter-chord line swept back 45°, with aspect ratio 4, taper ratio 0.6, and an NACA 65A006 airfoil section. Lift, drag, pitching moment, and root bending moment were obtained for the wing-alone and wing-body configurations. Effective downwash angles and dynamic-pressure characteristics in the region of the tail plane were also obtained and are presented for a range of tail heights at one tail length. The effects of two wing-fence arrangements were investigated. In order to expedite publishing of these data only a brief analysis is included.

INTRODUCTION

The urgent need for aerodynamic design data in the transonic speed range has led to the establishment of a special NACA committee for transonic research. As part of the NACA transonic research program recommended by this committee a series of wing-body configurations having wing plan form as the chief variable are being investigated in the Langley high-speed 7- by 10-foot tunnel utilizing the transonic-bump test technique. For each wing-fuselage combination investigated the lift, drag, pitching-moment, and root bending-moment characteristics are determined up to a Mach number of about 1.18. In addition, effective downwash angles and dynamic-pressure characteristics are obtained for a range of tail heights at one tail length.

This paper presents the results of the investigation of the wing-fuselage combination employing a wing with the quarter-chord line swept back 45°, with aspect ratio 4, taper ratio 0.6, and an NACA 65A006 airfoil section.

MODEL AND APPARATUS

The wing of the semispan model had 45° of sweepback referred to the quarter-chord line, a taper ratio of 0.60, aspect ratio of 4, and an NACA 65A006 airfoil section parallel to the free stream. The wing was made of beryllium copper and the fuselage of brass. A two-view drawing of the model is presented in figure 1 while ordinates of the fuselage of fineness ratio 10 can be found in table I. Details of the two wing fences that were used in the course of the investigation are shown in figure 2.

The model was mounted on an electrical strain-gage balance, which was enclosed in the bump, and the lift, drag, pitching moment, and bending moment about the model plane of symmetry were measured with calibrated galvanometers. The angle of attack was changed with a small electric motor and the value of the angle was determined with a calibrated slide-wire potentiometer.

Effective downwash angles were determined for a range of tail heights by measuring the floating angles of five free-floating tails with the aid of calibrated slide-wire potentiometers. Details of the floating tails, which had plan forms identical to that of the wing, are shown in figure 3; while a photograph of the test set-up on the bump is given in figure 4.

A total-head comb was used to determine dynamic-pressure ratios for a range of tail heights in a plane which contained the 25-percent mean-aerodynamic-chord point of the free-floating tails. The total-head tubes were spaced 0.25 inch apart.

SYMBOLS

C_L lift coefficient $\left(\frac{\text{Twice panel lift}}{qS}\right)$

C_D drag coefficient $\left(\frac{\text{Twice panel drag}}{qS}\right)$

C_m pitching-moment coefficient referred to $0.25\bar{c}$

$\left(\frac{\text{Twice panel pitching moment}}{qS\bar{c}}\right)$

C_B bending-moment coefficient at plane of symmetry $\left(\frac{\text{Root bending moment}}{q\left(\frac{S}{2}\right)\left(\frac{b}{2}\right)}\right)$

q effective dynamic pressure over span of model, pounds per square foot $\left(\frac{1}{2}\rho V^2\right)$

S twice wing area of semispan model, 0.1250 square foot

$\bar{c}$ mean aerodynamic chord of wing, 0.181 ft; based on relationship $\frac{2}{S}\int_0^{b/2} c^2 dy$ (using the theoretical tip)

c local wing chord

b twice span of semispan model

y spanwise distance from plane of symmetry

ρ air density, slugs per cubic foot

V airspeed, feet per second

M effective Mach number over span of model

M_a average chordwise local Mach number

M_l local Mach number

R Reynolds number of wing based on $\bar{c}$

α angle of attack, degrees

ϵ effective downwash angle, degrees

q_{wake}/q ratio of point dynamic pressure at quarter chord of tail mean aerodynamic chord to free-stream dynamic pressure

$(L/D)_{max}$ maximum ratio of lift to drag

y_{c_p} lateral center of pressure, percent semispan $\left(100C_B/C_L\right)$

h_t tail height relative to wing chord plane extended, percent semispan; positive for tail positions above the chord plane extended

Subscripts and abbreviations:

W	wing
WF	wing-fuselage
a.c.	aerodynamic center

TESTS

The tests were made in the Langley high-speed 7- by 10-foot tunnel utilizing an adaptation of the NACA wing-flow technique for obtaining transonic speeds. The technique used involves placing the model in the high-velocity flow field generated over the curved surface of a bump on the tunnel floor. (See reference 1.)

Typical contours of local Mach number in the vicinity of the model location on the bump are shown in figure 5. These data show that there is a Mach number gradient of about 0.04 over the inboard semispan at low Mach numbers and from 0.06 to 0.07 at the highest Mach numbers. The chordwise Mach number gradient is generally less than 0.01. No attempt has been made to evaluate the effects of this chordwise and spanwise Mach number variation. Note that the long dashed lines shown near the root of the wing (fig. 5) indicate a local Mach number 5 percent below the maximum value and represent a nominal extent of the bump boundary layer. The effective test Mach number was obtained from contour charts similar to those presented in figure 5 using the relationship

$$M = \frac{2}{S}\int_0^{b/2} cM_a dy$$

The variation of mean test Reynolds number with Mach number is shown in figure 6. The boundaries on the figure are an indication of the probable range in Reynolds number caused by variations in test conditions in the course of the investigation.

Force and moment data, effective downwash angles, and the ratio of dynamic pressure at 25 percent of the tail mean aerodynamic chord to free-stream dynamic pressure were obtained for various model configurations through a Mach number range of 0.60 to 1.18 and an angle-of-attack range of -2° to 10°.

No tares have been applied to the data to account for the presence of the end plates on the models. Jet-boundary corrections have not been evaluated because the boundary conditions to be satisfied are not rigorously defined. However, inasmuch as the effective flow field is large compared with the span and chord of the model the corrections are believed to be small.

By measuring tail floating angles without a model installed it was determined that a tail spacing of 2 inches would produce negligible interference effects of reflected shock waves on the tail floating angles. Downwash angles for the wing-alone configuration were therefore obtained simultaneously for the middle, highest, and lowest tail positions in one series of tests, and simultaneously for the two intermediate positions in succeeding runs. (See fig. 3.) The downwash angles presented are increments from the tail floating angles without a model in position. It should be noted that the floating angles measured are in reality a measure of zero pitching moment about the tail pivot axis rather than the angle of zero lift. It has been estimated, however, that for the tail arrangement used a downwash gradient of 2° across the span of the tail will result in an error of less than 0.1° in the measured downwash angle.

Total-head readings obtained from the tail survey comb have been corrected for bow wave loss. The static-pressure values used in computing the dynamic-pressure ratios were obtained by use of a static probe.

RESULTS AND DISCUSSION

A table of the figures presenting the results is given below:

	Figure
Basic wing-alone data	7
Basic wing-fuselage data	8
Effect of wing fences on wing-fuselage characteristics	9
Dynamic-pressure surveys	10
Effective downwash angles (wing alone)	11
Effective downwash angles (wing fuselage)	12
Summary of aerodynamic characteristics	13

The discussion is based on the summarized values given in figure 13 unless otherwise noted. Note that the slopes summarized in figure 13 have been averaged over a lift range of ± 0.1 of the nominal lift coefficient.

Lift and Drag Characteristics

The wing-alone lift-curve slope measured near zero lift was about 0.059 at a Mach number of 0.60. This compared with $\partial C_L/\partial \alpha$ of 0.057 obtained from the unpublished low-speed semispan data of a wing with identical geometry which was tested in the Langley two-dimensional tunnel at Reynolds numbers up to 12×10^6. The lift curves below $M = 1.05$ were nonlinear; the slope at higher lift coefficients was somewhat less than that near zero lift. Above $M = 1.05$ the lift curves were essentially

linear over the test lift range. (See figs. 7 and 13.) The basic lift-curve slope was increased by an average of 20 percent by the addition of the fuselage.

The drag rise at zero lift occurred at a Mach number of about 0.93 for both wing and wing-fuselage conditions. It should be remembered that the absolute drag coefficients are probably high because of the presence of end-plate tare and also because of the low Reynolds numbers at which the tests were run. At a Mach number of 0.6 the minimum drag coefficient for the wing alone was 0.010. This value compares with a minimum drag value of approximately 0.0050 obtained from the previously mentioned low-speed investigation made at a Reynolds number of 12×10^6. The values of $(L/D)_{max}$ shown in figure 13 are somewhat low because of high absolute drag and are presented primarily for comparison with the other wings to be investigated in this series.

The lateral center of pressure for the wing alone $(C_L = 0.4)$ increased from about 48 percent semispan at $M = 0.60$ to about 50 percent semispan at $M = 0.98$. Between $M = 0.98$ and 1.05 there is a fairly abrupt outboard movement of y_{c_p} to about 55 percent of the semispan. The addition of the fuselage moved the lateral center of pressure inboard an average of about 3 percent semispan throughout the Mach number range.

Pitching-Moment Characteristics

Near zero lift coefficient, the wing aerodynamic center was about 32 percent mean aerodynamic chord and was almost constant throughout the Mach number range. This value compares with a low-speed aerodynamic-center location of 25 percent mean aerodynamic chord near zero lift obtained from the unpublished Langley two-dimensional-tunnel data. The addition of the fuselage moved the aerodynamic center forward about 7 percent mean aerodynamic chord below $M = 1.00$ and forward to a lesser extent at the higher Mach numbers. At $C_L = 0.4$ the wing-alone aerodynamic center varied from about 22 percent mean aerodynamic chord at low Mach numbers to 45 percent mean aerodynamic chord at $M = 1.18$. The unstable shift in aerodynamic center at low Mach numbers in the higher C_L range is even more pronounced for the wing-fuselage condition.

Effect of Wing Fences

In an attempt to alleviate the unstable aerodynamic-center shift, which was probably caused by premature flow separation at the tip in the higher lift range at low Mach numbers, it was decided to investigate two upper-surface wing fences on the wing-fuselage combination.

It would appear that the use of either fence would reduce the severity of the unstable aerodynamic-center shift considerably at low Mach numbers. (See fig. 9.) Note also that with a wing fence the stabilizing aerodynamic-center shift at $M = 1.10$ is reduced considerably, and y_{c_p} does not vary appreciably with Mach number. The fences produced only minor effects on the lift and drag characteristics. (See fig. 9.)

Downwash and Dynamic-Pressure Surveys in Region of Tail Plane

The variation of isolated wing effective downwash angle with tail height and angle of attack for various Mach numbers are presented in figure 11. There is a fairly small effect of tail height and Mach number on $\partial\epsilon/\partial\alpha$ near zero lift for a tail location between 30 percent semispan above or below the wing chord line extended. (See fig. 13). At the higher lift coefficients the variations of $\partial\epsilon/\partial\alpha$ appear more erratic, but there appears to be a marked decrease in $\partial\epsilon/\partial\alpha$ for all tail locations at the highest test Mach numbers. (See fig. 11).

The results of limited downwash data obtained for the wing-fuselage condition are presented in figure 12. For angles of attack greater than 4° it was not possible to obtain data for the two innermost vane positions because of fuselage interference. The dashed curves in the region of the chord line extended have been estimated from unpublished results obtained for other models of this series with a free-floating tail mounted on the fuselage center line.

The results of point dynamic-pressure surveys, made in a plane perpendicular to the chord plane extended at $\alpha = 0^\circ$ and containing the 25-percent mean-aerodynamic-chord point of the free-floating tails used in the downwash surveys, indicate that the loss in free-stream dynamic pressure was almost always less than 10 percent up to $M = 1.15$ regardless of tail height. (See figs. 10 and 13.)

Langley Aeronautical Laboratory
National Advisory Committee for Aeronautics
Langley Air Force Base, Va.

REFERENCE

1. Schneiter, Leslie E., and Ziff, Howard L.: Preliminary Investigation of Spoiler Lateral Control on a 42° Sweptback Wing at Transonic Speeds. NACA RM No. L7F19, 1947.

TABLE I.- FUSELAGE ORDINATES

[Basic fineness ratio 12; actual fineness ratio 10 achieved by cutting off the rear one-sixth of the body; $\bar{c}/4$ located at $l/2$]

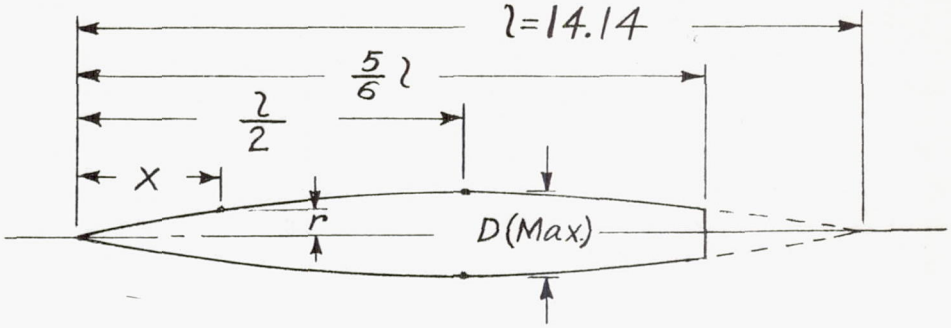

Ordinates			
x/l	r/l	x/l	r/l
0	0	0	0
.005	.00231	.4500	.04143
.0075	.00298	.5000	.04167
.0125	.00428	.5500	.04130
.0250	.00722	.6000	.04024
.0500	.01205	.6500	.03842
.0750	.01613	.7000	.03562
.1000	.01971	.7500	.03128
.1500	.02593	.8000	.02526
.2000	.03090	.8338	.02000
.2500	.03465	.8500	.01852
.3000	.03741	.9000	.01125
.3500	.03933	.9500	.00439
.4000	.04063	1.0000	0
L. E. radius = 0.00051			

NACA

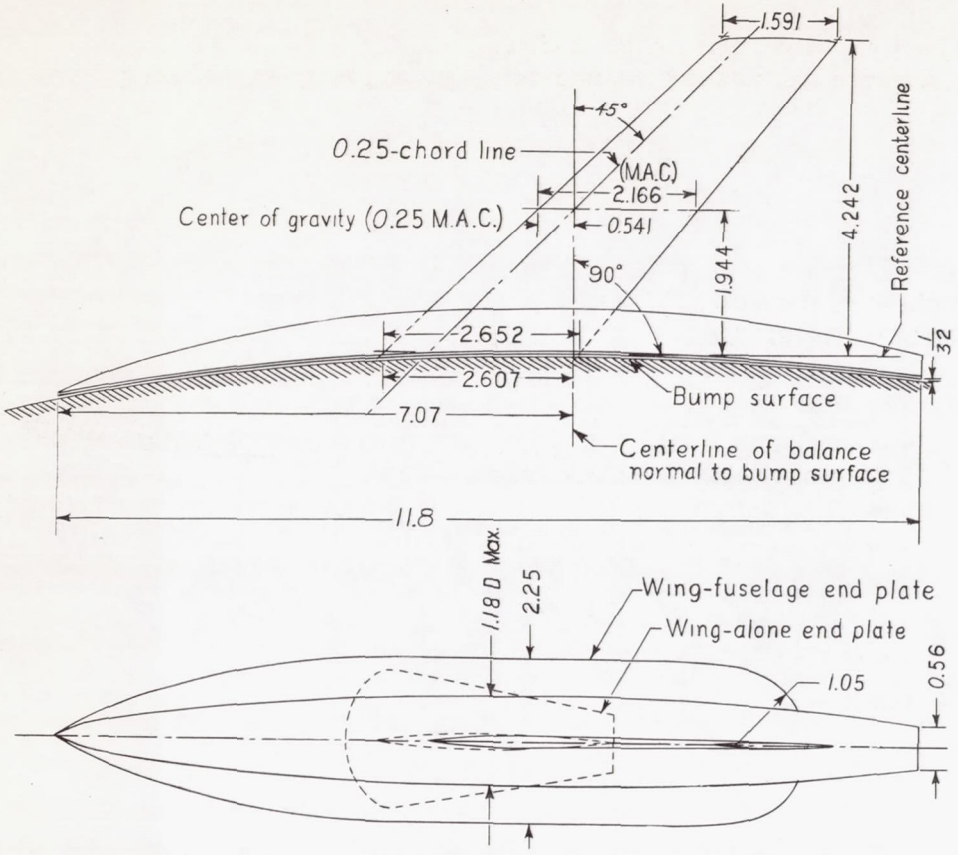

TABULATED DATA

Wing

Twice semispan area	0.125 sq ft
Aspect ratio	4.0
Taper ratio	0.60
Mean aerodynamic chord	0.180 ft
Incidence	0°
Dihedral	0°
Airfoil section parallel to free airstream	NACA 65A006

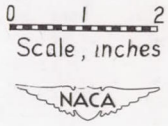

Figure 1.– General arrangement of model with 45° sweptback wing, aspect ratio 4, taper ratio 0.6, and NACA 65A006 airfoil.

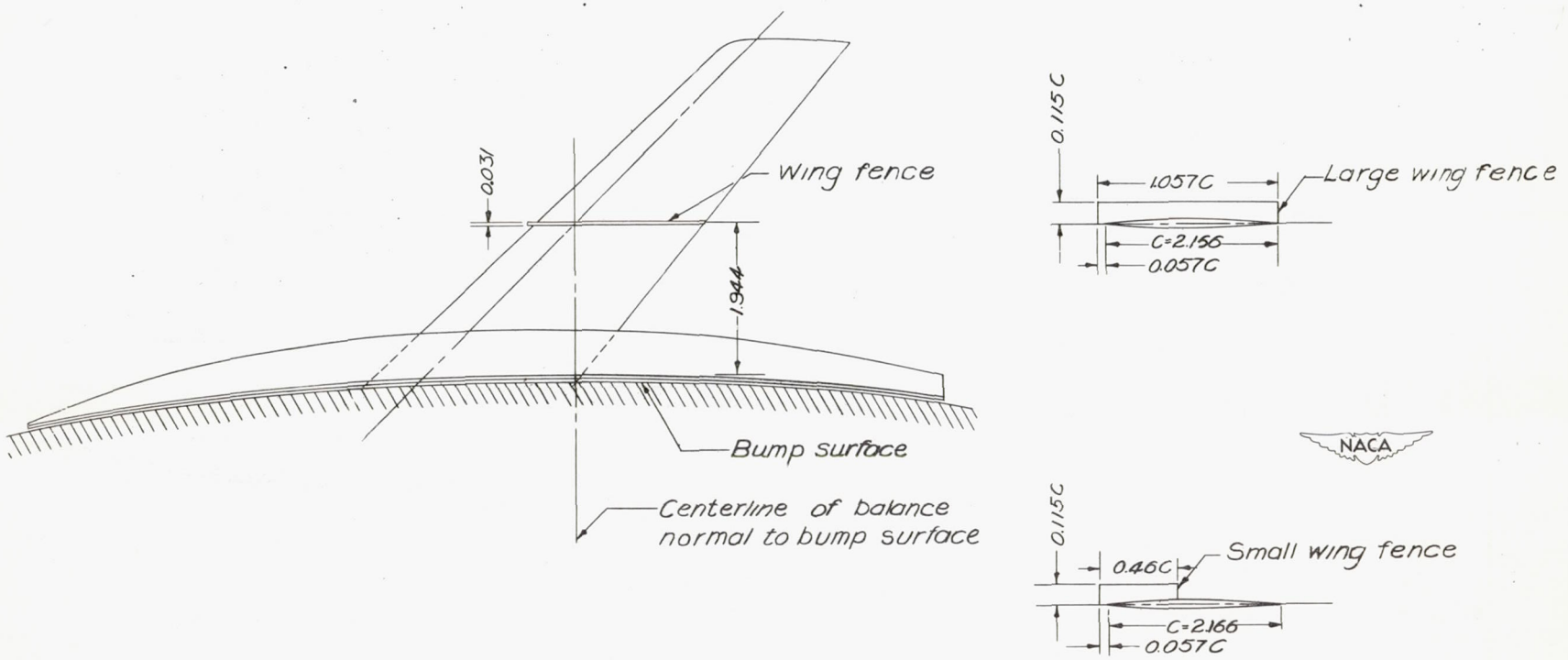

Figure 2.– Details of wing fences tested on model with 45° sweptback wing, aspect ratio 4, taper ratio 0.6, and NACA 65A006 airfoil.

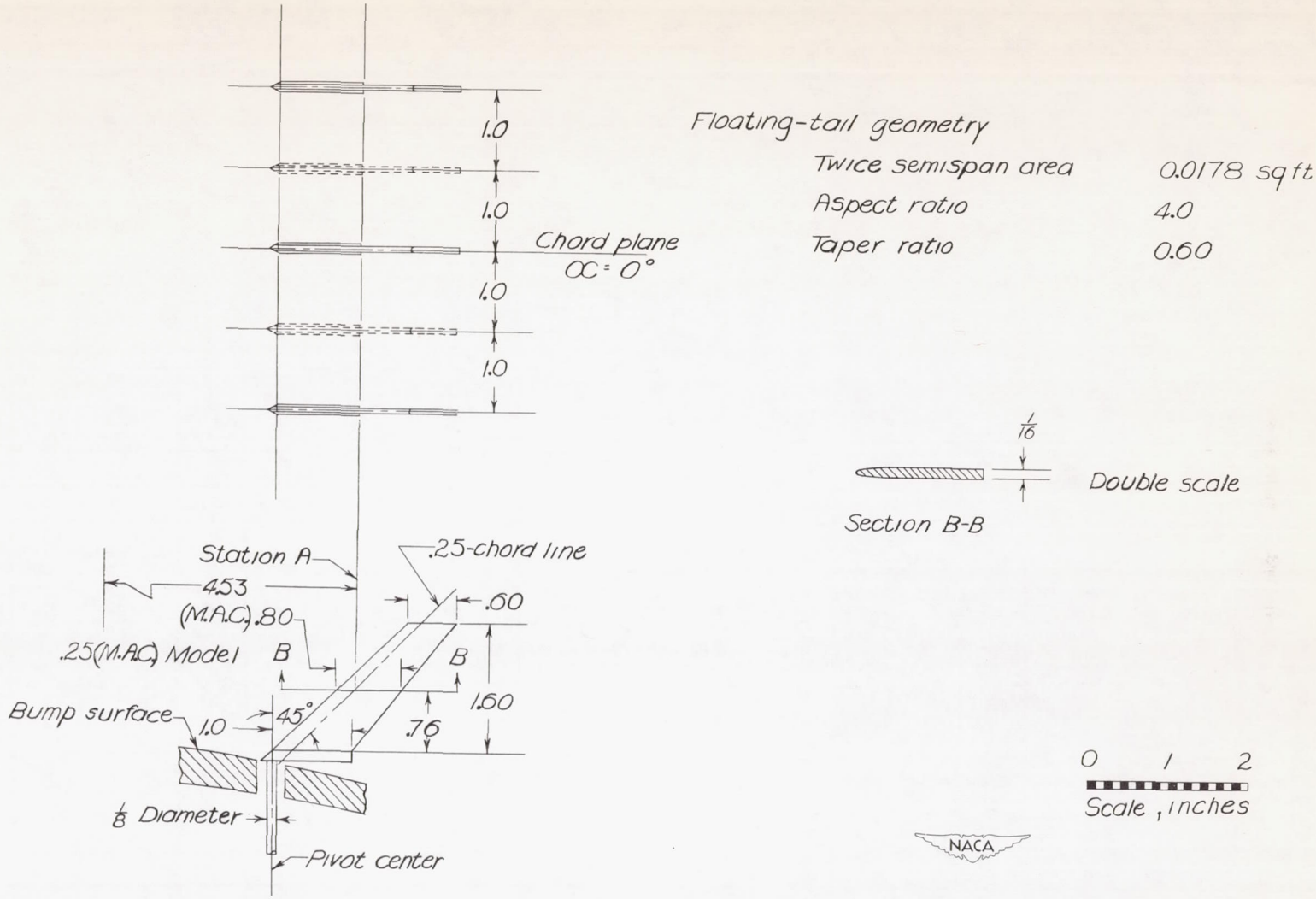

Figure 3.– Details of free–floating tails used in surveys behind model with 45° sweptback wing, aspect ratio 4, taper ratio 0.6, and NACA 65A006 airfoil.

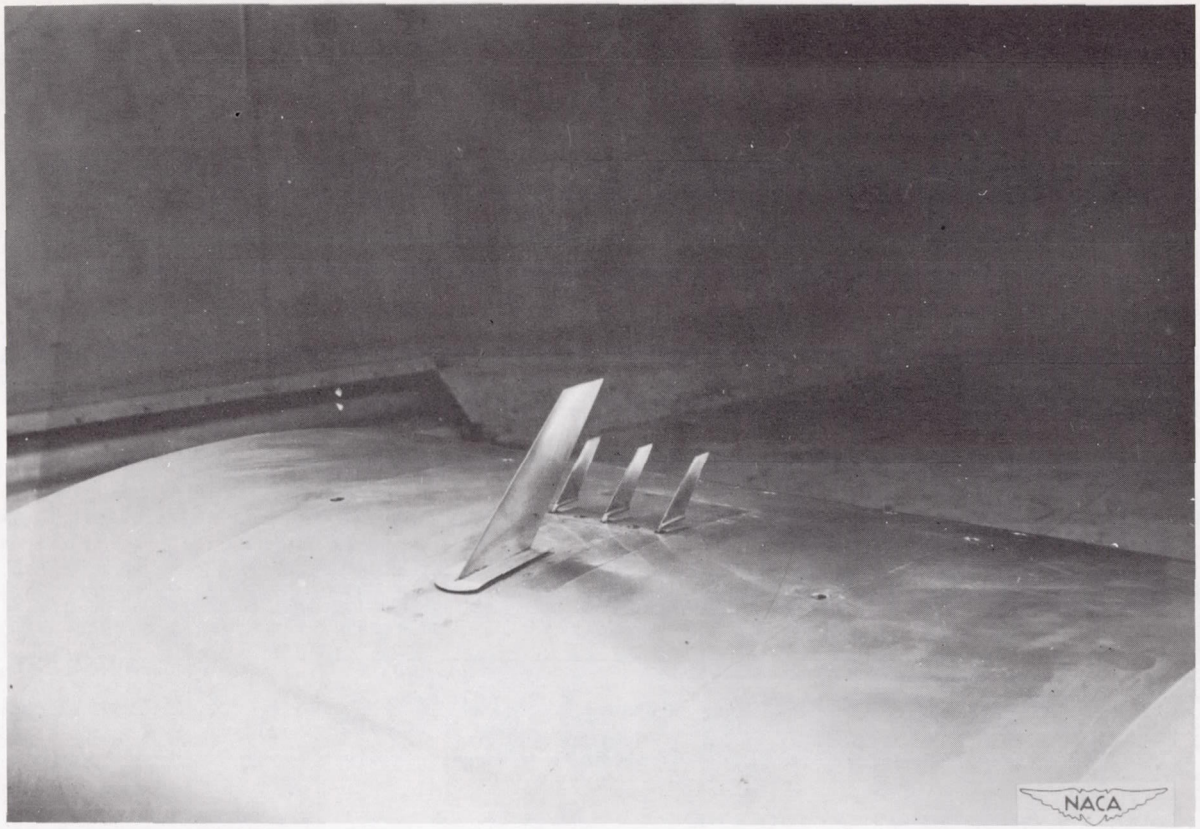

Figure 4.– Photograph of model with 45° sweptback wing, aspect ratio 4, taper ratio 0.6, and NACA 65A006 airfoil showing free–floating tails.

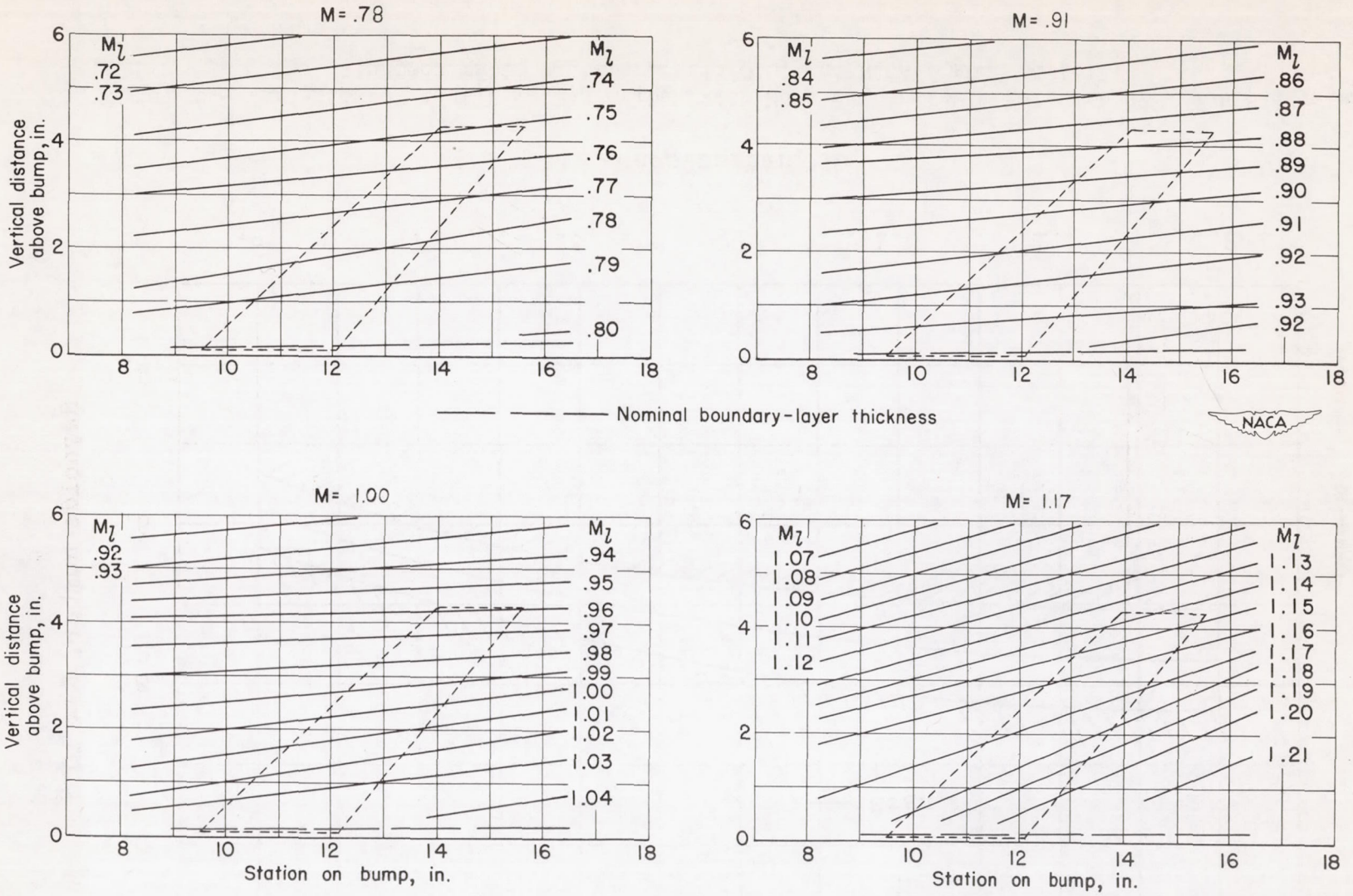

Figure 5.- Typical Mach number contours over transonic bump in region of model location.

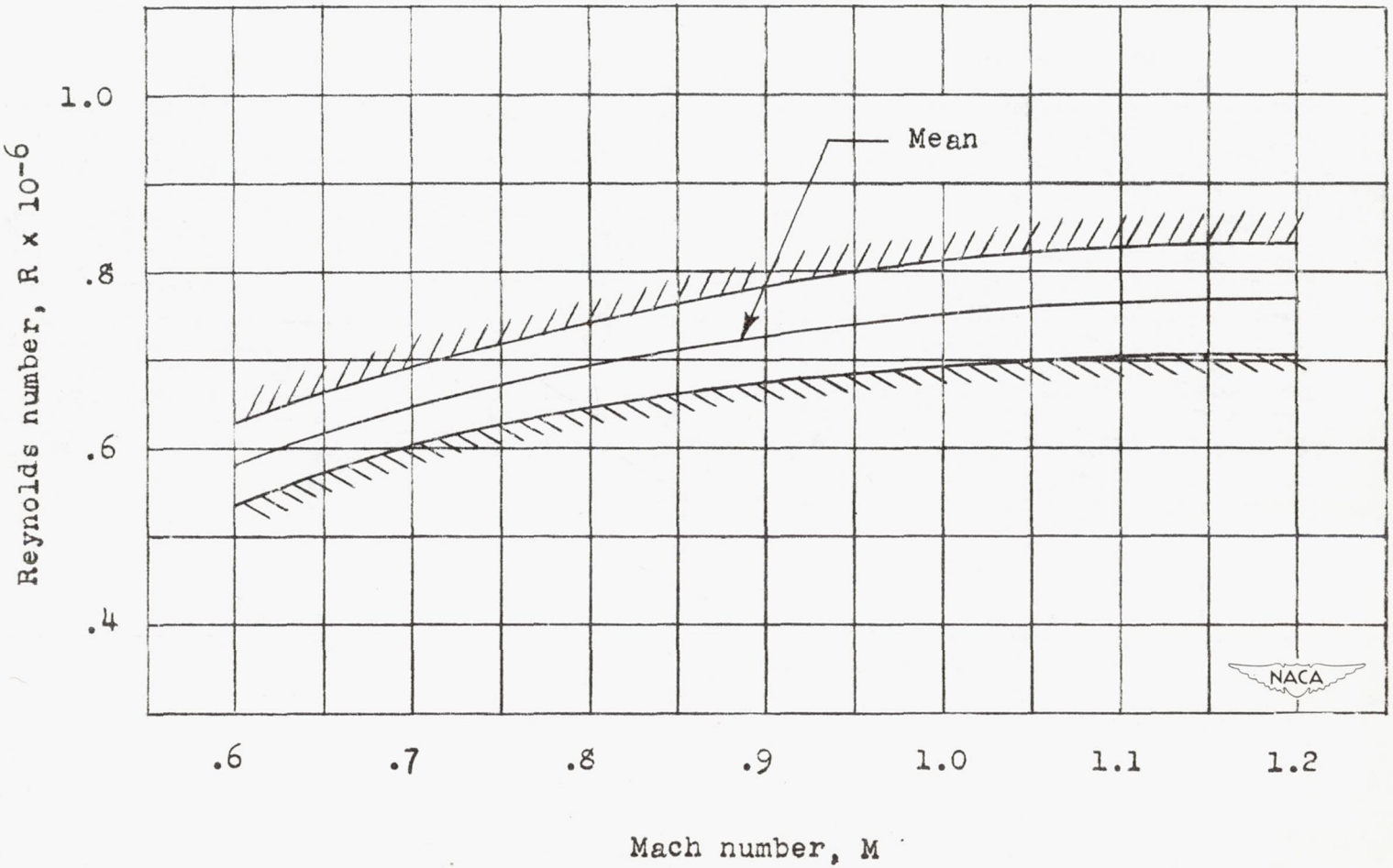

Figure 6.– Variation of test Reynolds number with Mach number for model with 45° sweptback wing, aspect ratio 4, taper ratio 0.6, and NACA 65A006 airfoil.

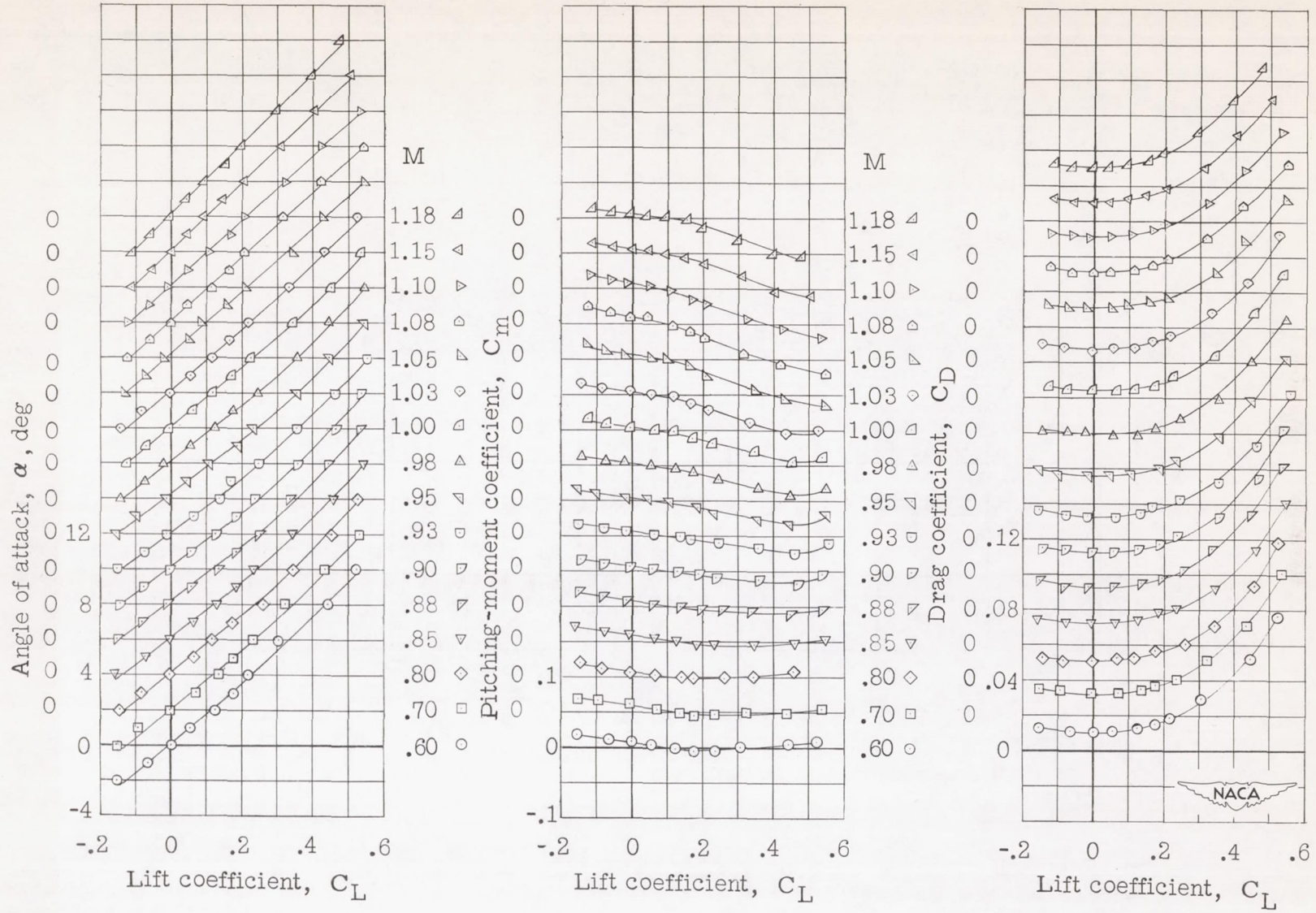

Figure 7.– Wing–alone aerodynamic characteristics for model with 45° sweptback wing, aspect ratio 4, taper ratio 0.6, and NACA 65A006 airfoil.

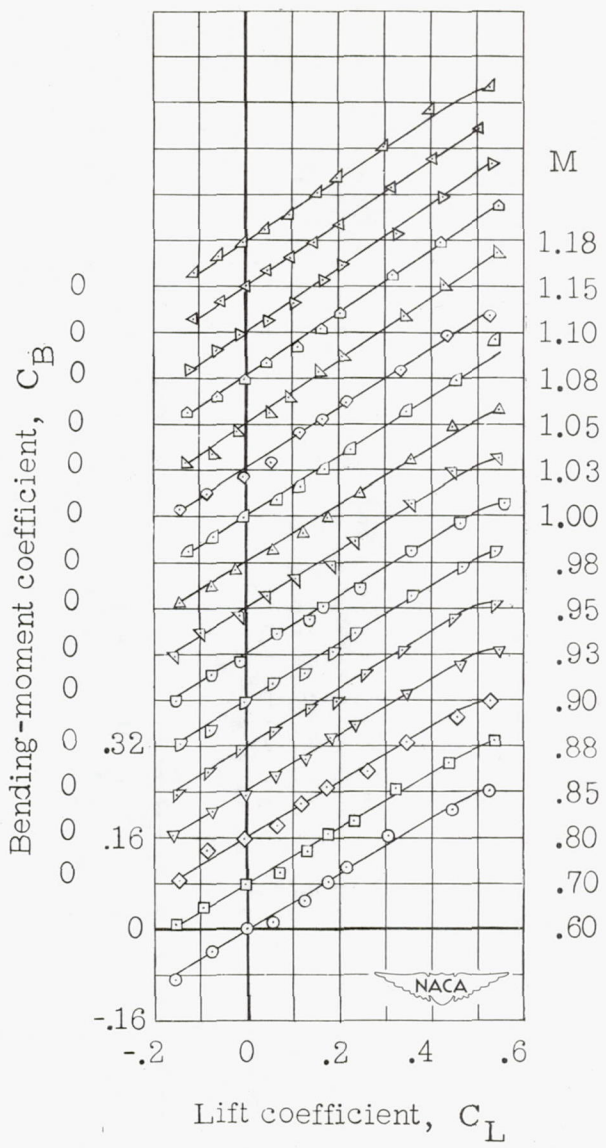

Figure 7.– Concluded.

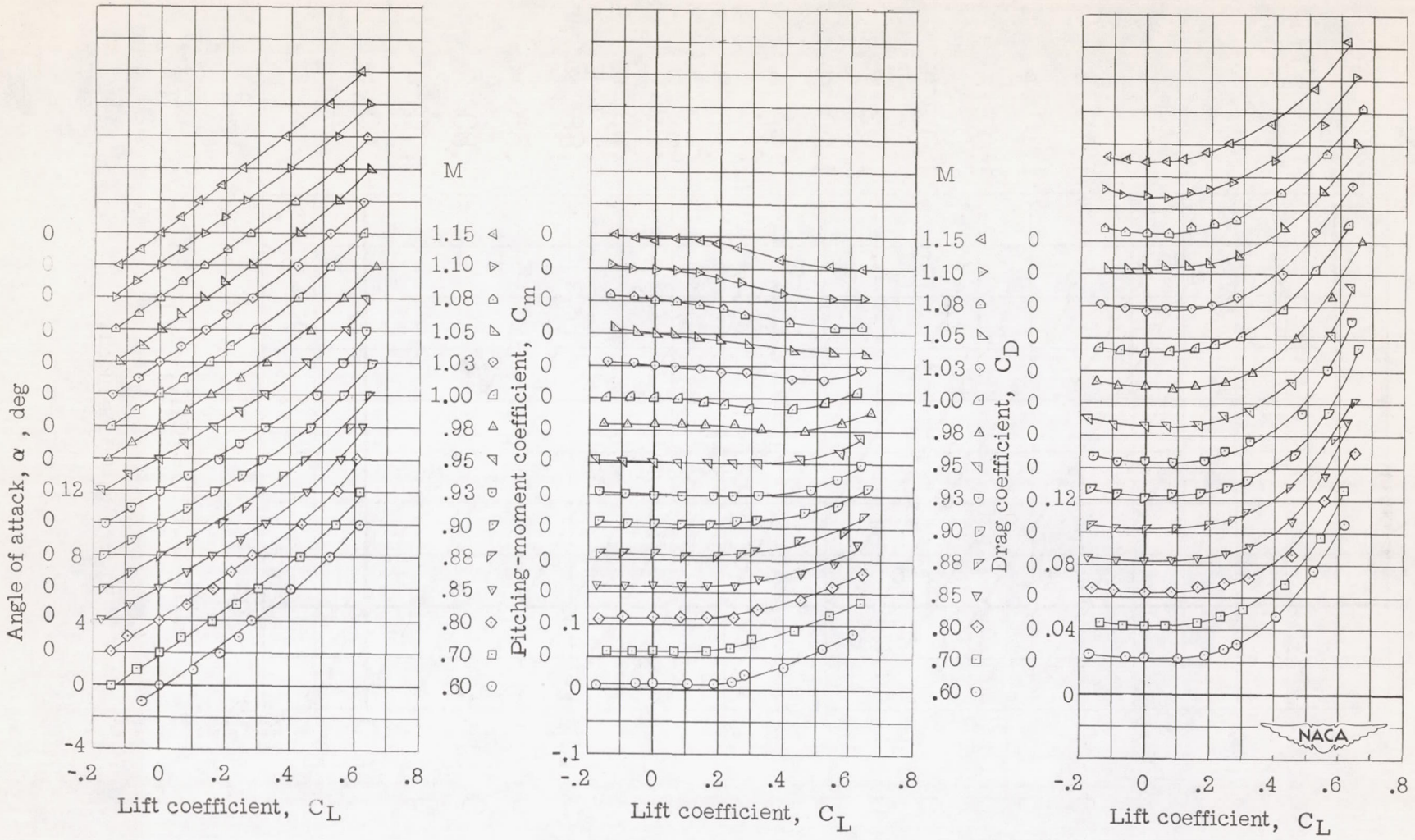

Figure 8.- Wing-fuselage aerodynamic characteristics for model with 45° sweptback wing, aspect ratio 4, taper ratio 0.6, and NACA 65A006 airfoil.

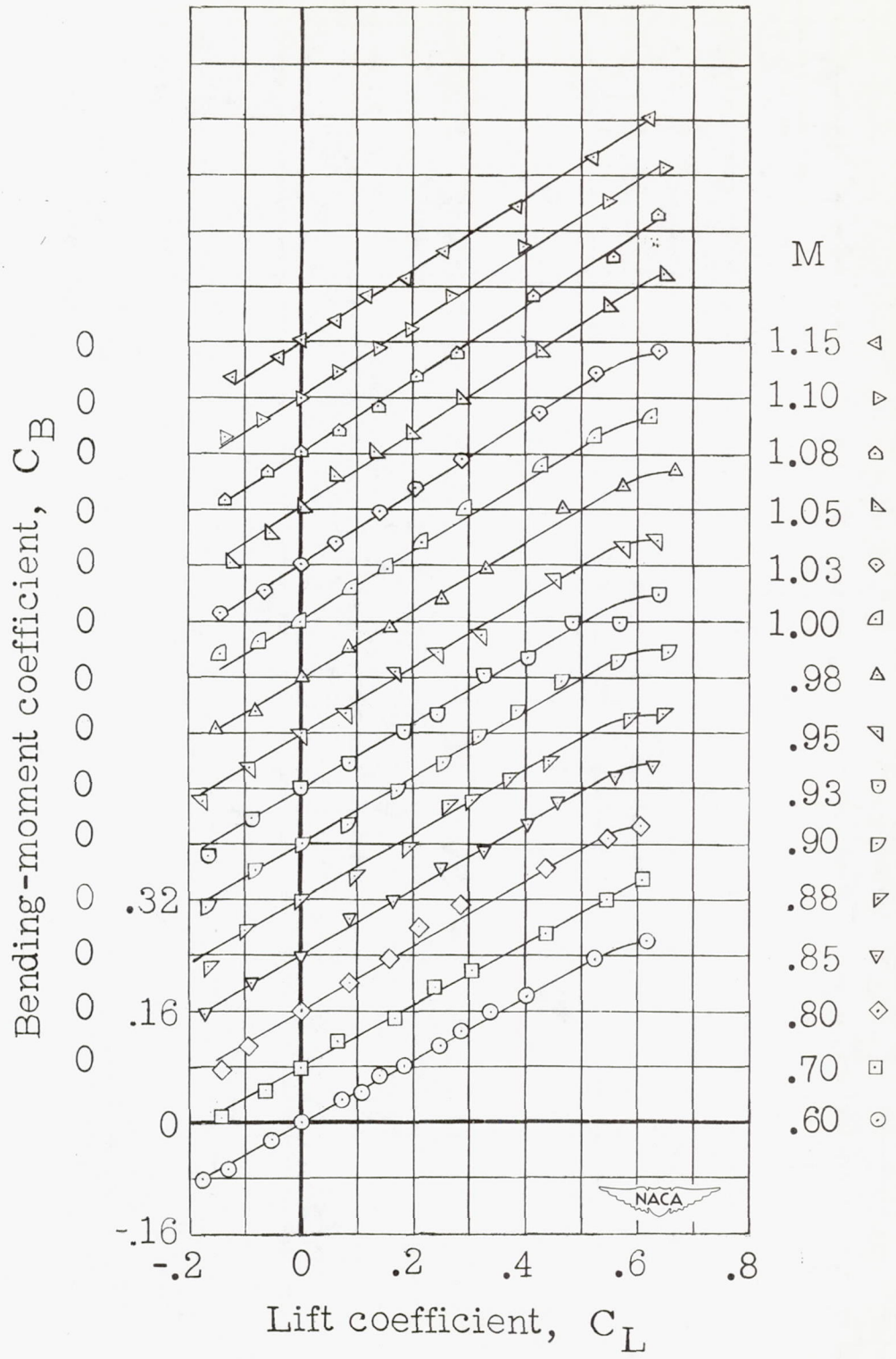

Figure 8.– Concluded.

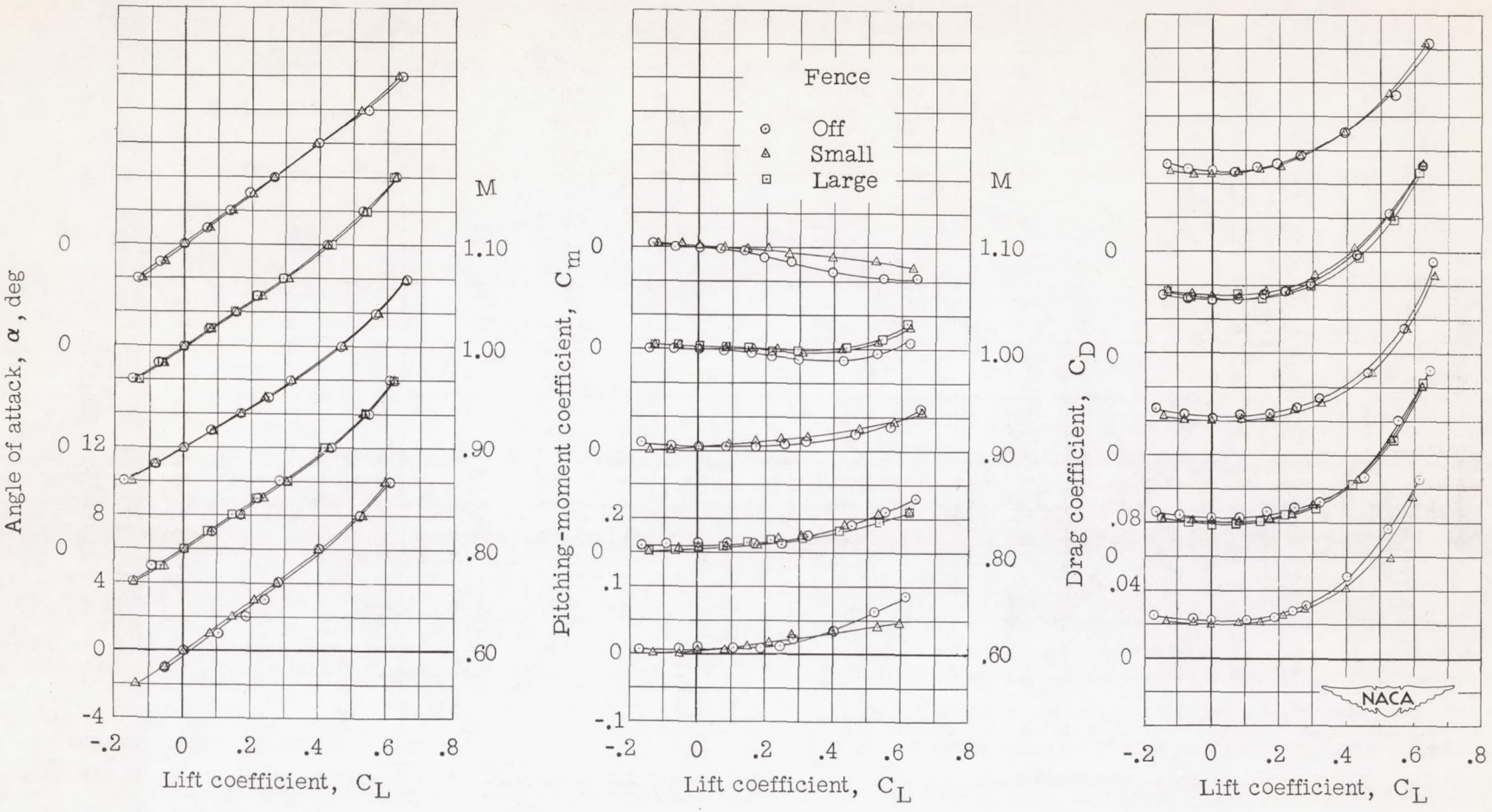

Figure 9.– Effect of wing fences on the wing–fuselage aerodynamic characteristics for a model with 45° sweptback wing, aspect ratio 4, taper ratio 0.6, and NACA 65A006 airfoil.

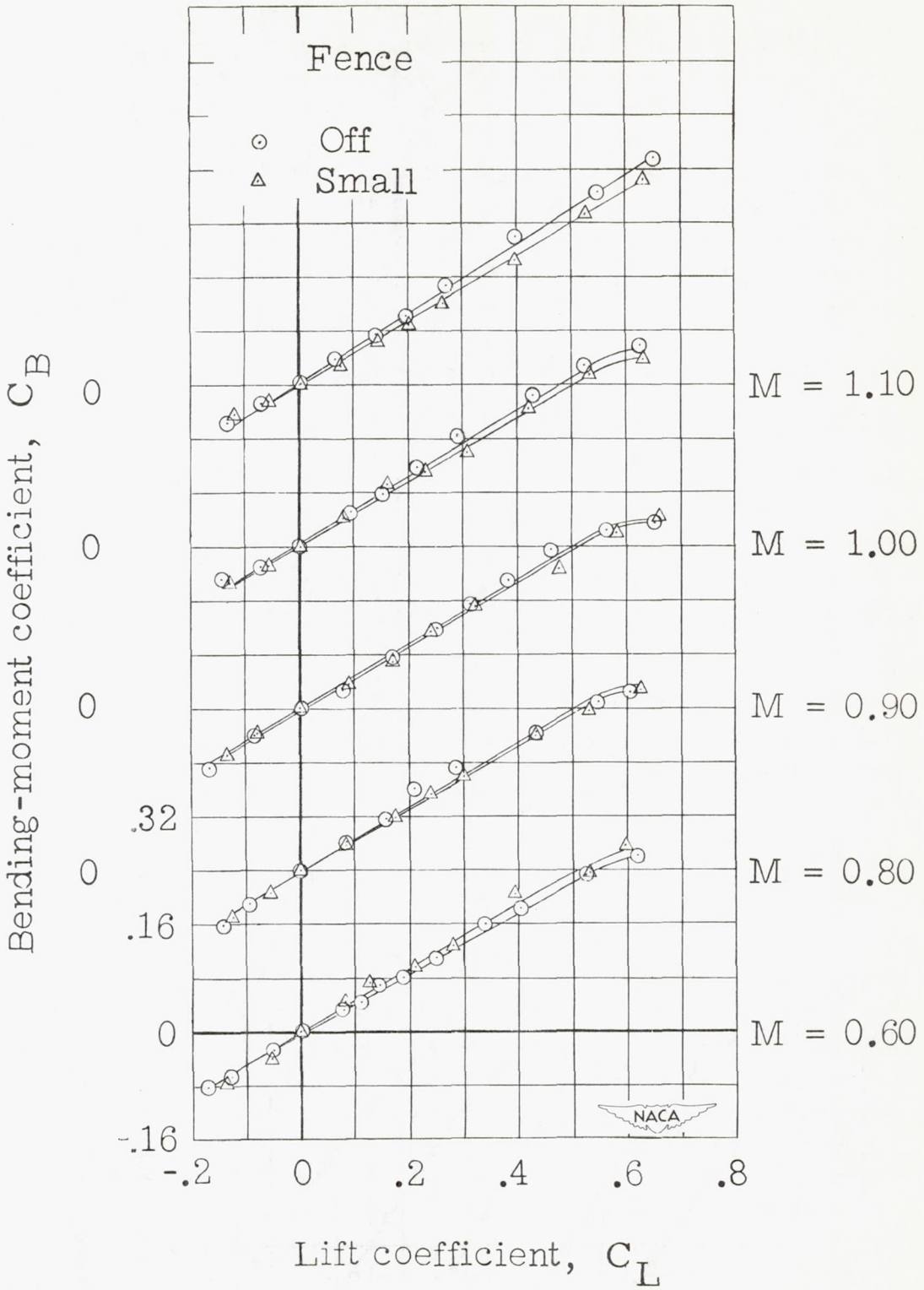

Figure 9.– Concluded.

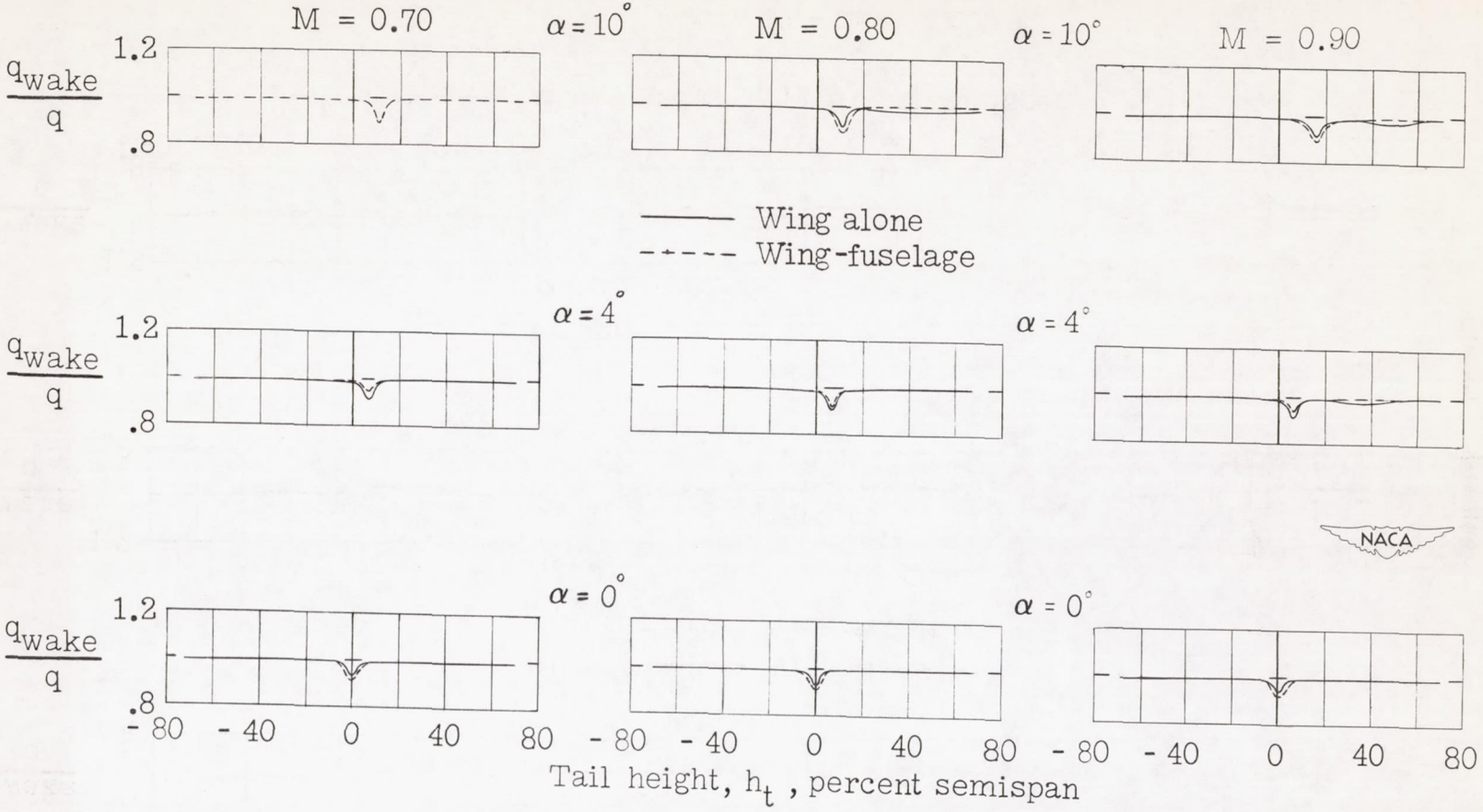

Figure 10.— Dynamic-pressure surveys in region of tail plane for a model with 45° sweptback wing, aspect ratio 4, taper ratio 0.6, and NACA 65A006 airfoil.

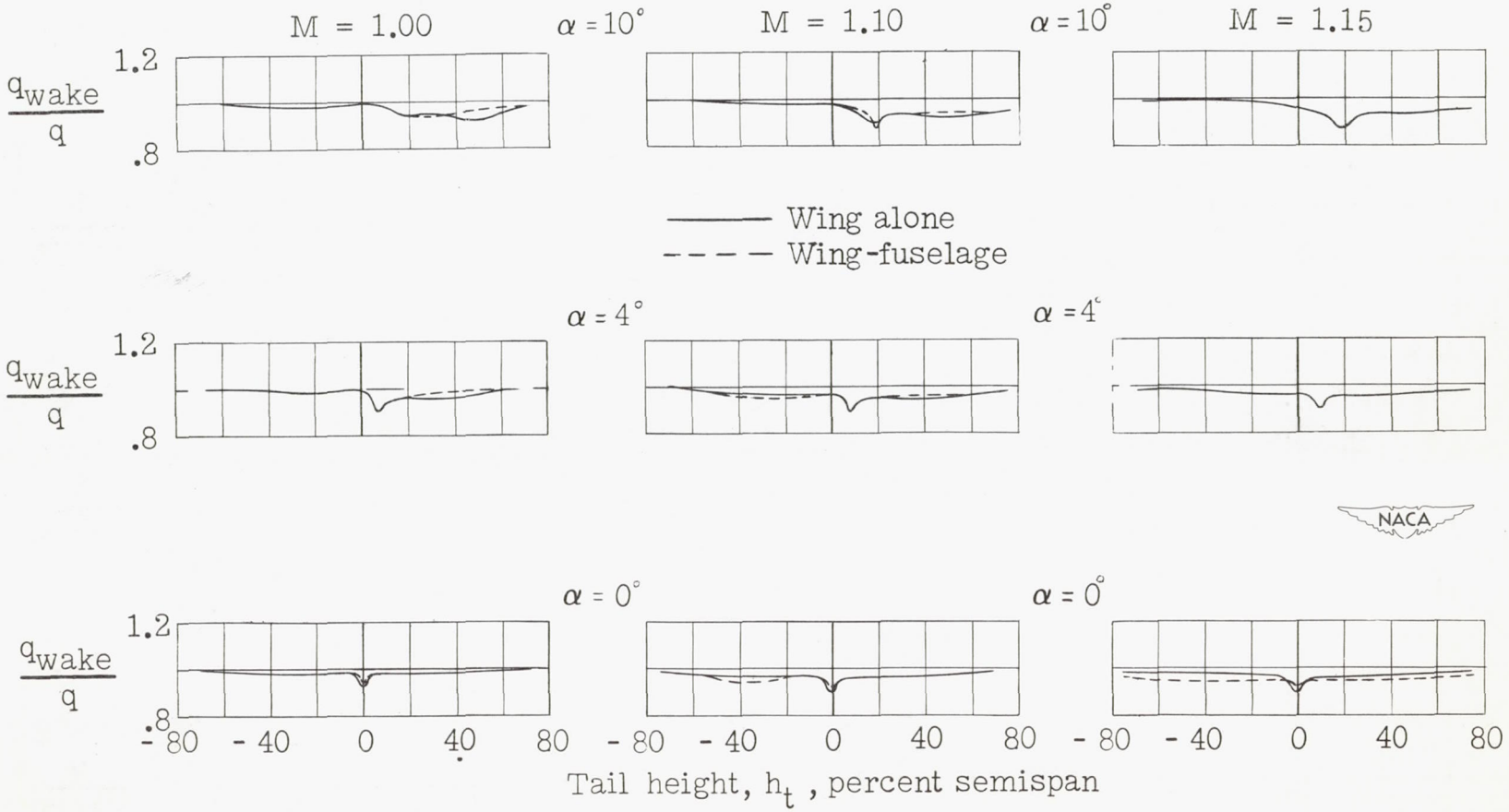

Figure 10.– Concluded.

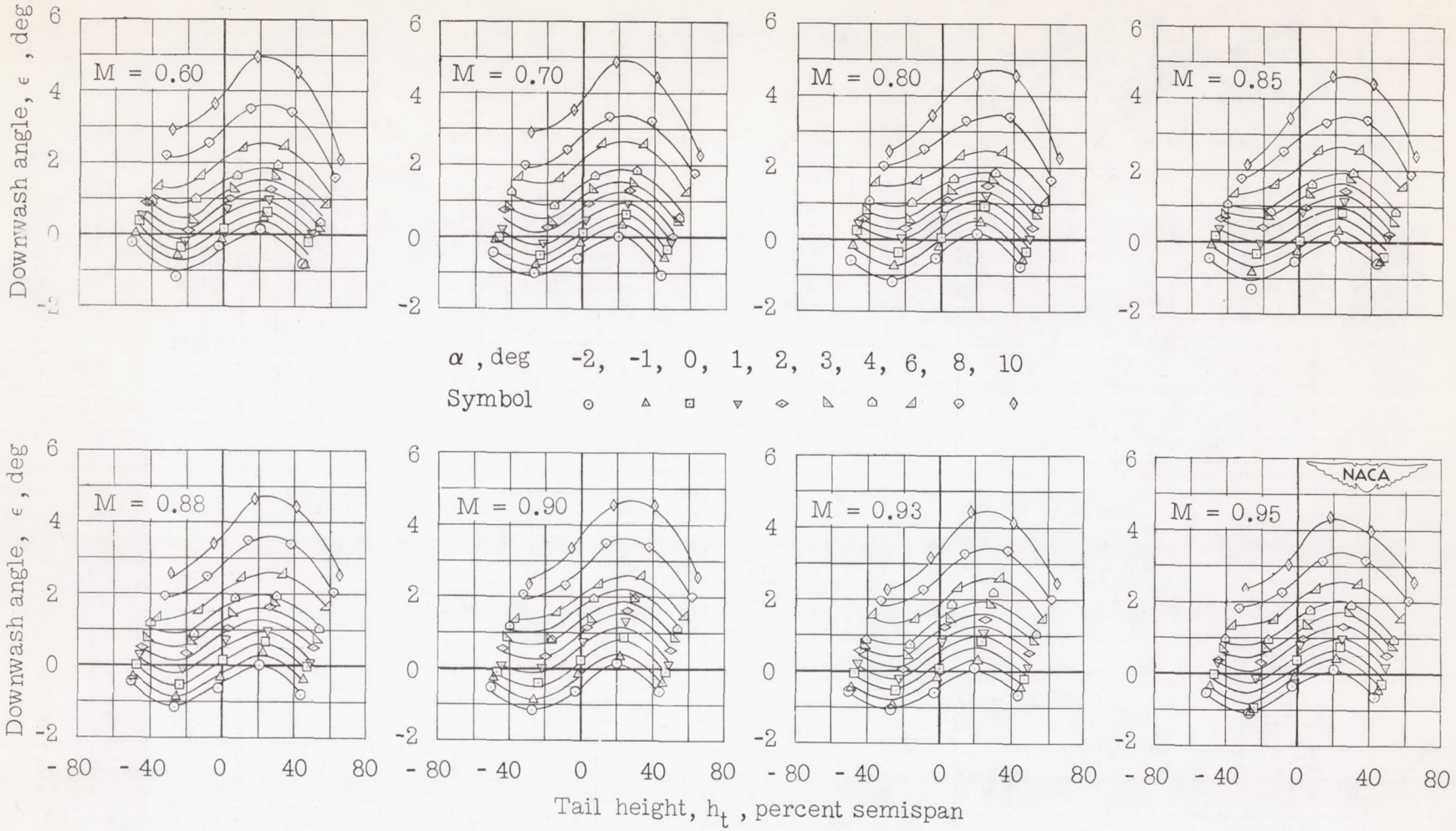

Figure 11.– Effective downwash angles in region of tail plane for a model with 45° sweptback wing, aspect ratio 4, taper ratio 0.6, and NACA 65A006 airfoil. Wing alone.

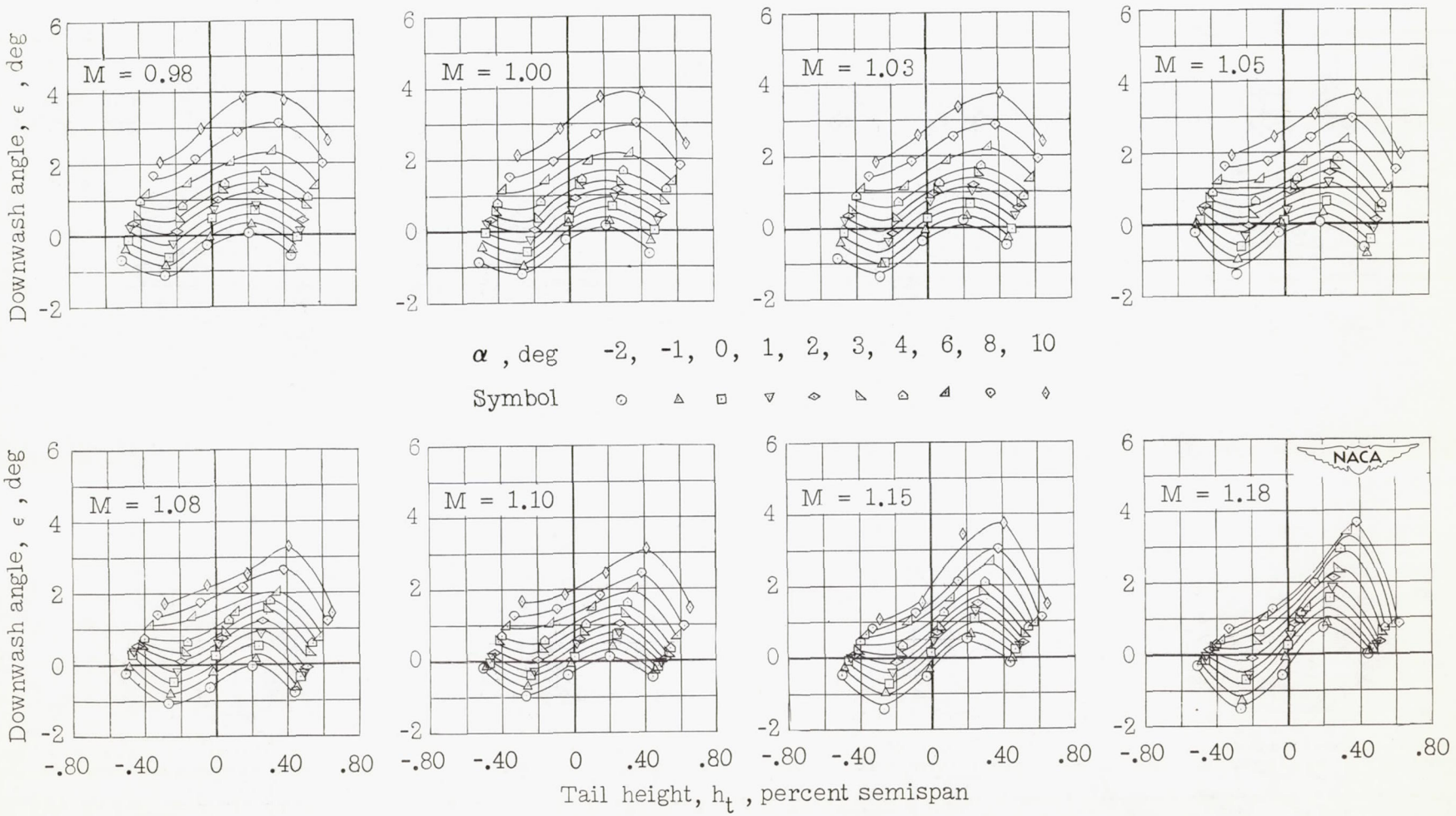

Figure 11.– Concluded.

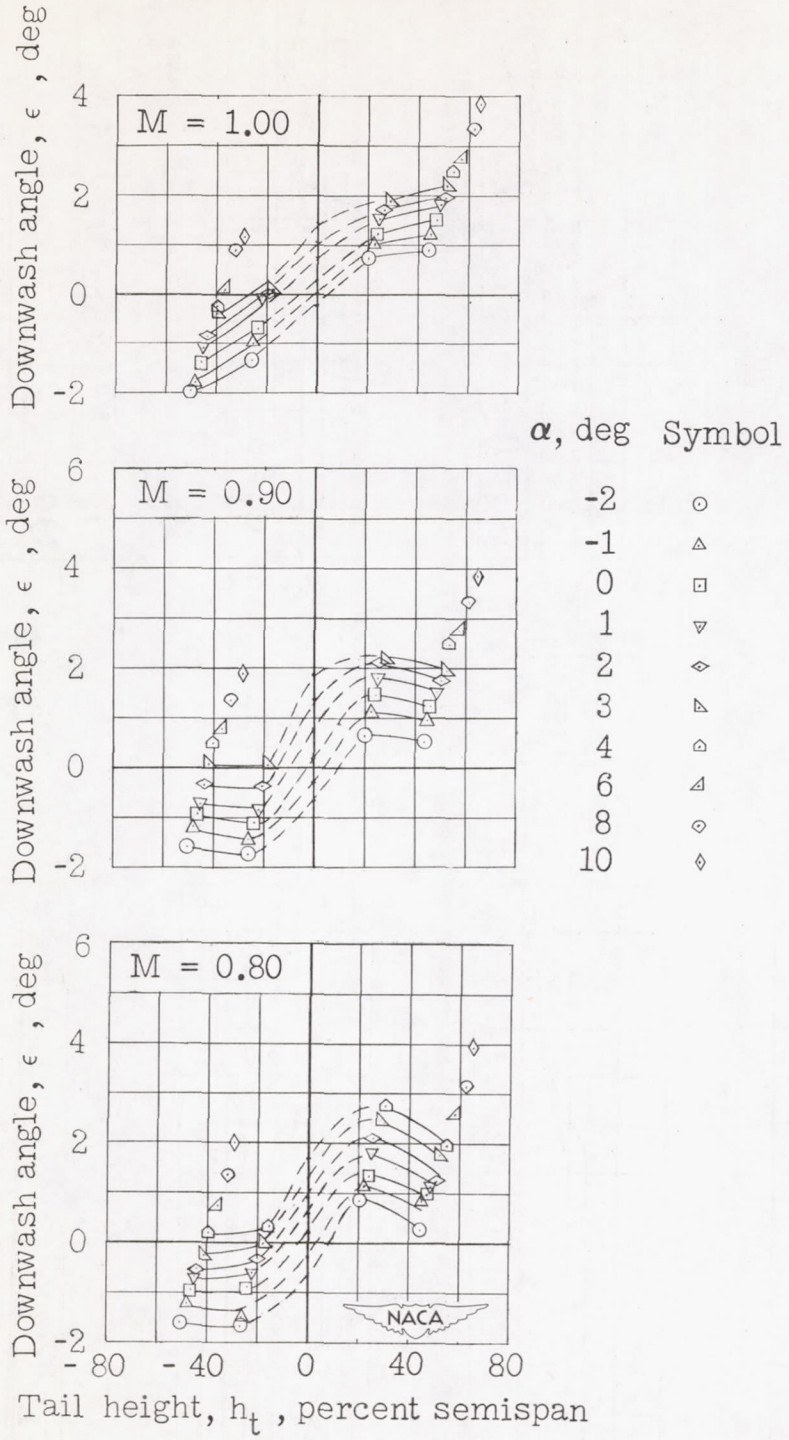

Figure 12.– Effective downwash angles in region of tail plane for a model with 45° sweptback wing, aspect ratio 4, taper ratio 0.6, and NACA 65A006 airfoil. Wing fuselage.

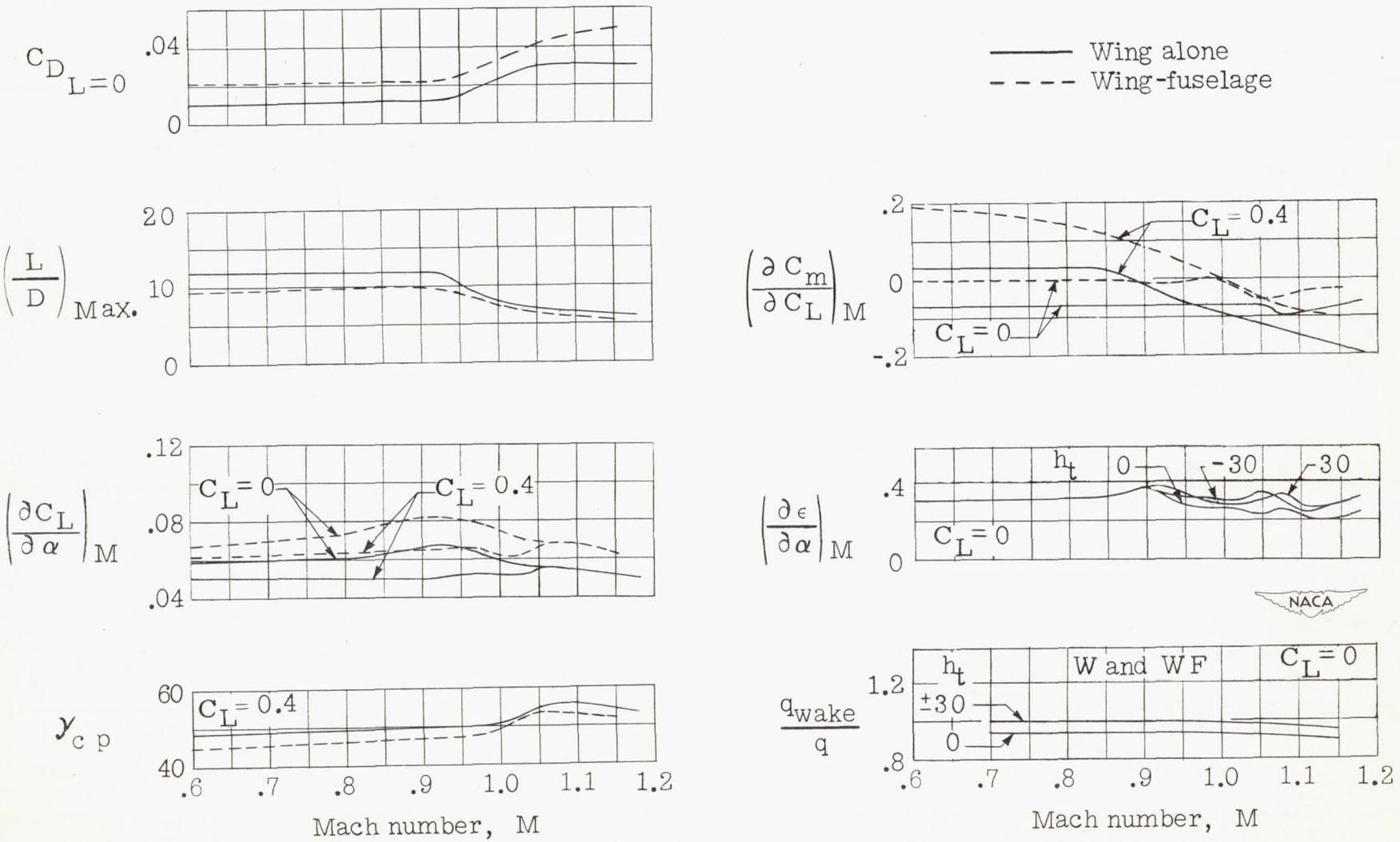

Figure 13.– Summary of aerodynamic characteristics for a model with 45° sweptback wing, aspect ratio 4, taper ratio 0.6, and NACA 65A006 airfoil.